PCCP

ARTICLE

Dynamics of π*-resonances in anionic clusters of *para*-toluquinone

Received 00th January 20xx,
Accepted 00th January 20xx

DOI: 10.1039/x0xx00000x

www.rsc.org/

James N. Bull[a,b] and Jan R. R. Verlet[a]

Frequency-resolved photoelectron spectroscopy applied to mass-selected cluster anions is an insightful approach to characterise the dynamics of π*-resonances with microsolvation. Here, the technique demonstrated with monomer, dimer and trimer radical anions of *para*-toluquinone (pTQ) over a ~1 eV excitation window above the detachment threshold. The pTQ^- spectra show similar resonances and dynamics to *para*-benzoquinone, a prototype electrophore. The dimer, $(pTQ)_2^-$, has a π-stacked geometry and shows a competition between photodissociation and prompt autodetachment. The trimer, $(pTQ)_3^-$, also has a π-stacked cluster geometry and shows vibrational autodetachment from a non-valence state up to ~0.7 eV above-threshold, outcompeting dissociation. At higher photoexcitation energies, $(pTQ)_3^-$ shows monomer-like dynamics, blue-shifted in photoexcitation energy by the cluster cohesion energy. Overall, the study highlights the variety of non-adiabatic dynamics available to π*-resonances and the profound changes that occur through clusterization with one and two monomers.

Introduction

The properties, spectroscopy and dynamics of short-lived anions such as above-threshold resonances,[1,2] dipole-bound states,[1,3] and non-valence correlation-bound states has been the subject of much interest over the last few decades.[4] The dynamics of such states are difficult to probe directly because the lifetime of anion resonances are typically shorter than 100 fs while non-valence states usually live for picoseconds. Similarly, from a computational perspective, rigorous theoretical treatments of resonances and their dynamics are challenging.[5,6] Over the past few years, the rich non-adiabatic coupling and dynamics between anionic excited states of both valence and non-valence type and the detachment continuum have been conveniently explored using time-resolved and frequency-resolved photoelectron imaging.[7-13]

Advancing an understanding of resonance dynamics in an interacting or condensed phase environment can be approached by studying the evolution of dynamics from the isolated anion (gas-phase) to the anion embedded in a cluster.[14] Increasing cluster size leads to an increase in the number and density of states and product channels, often limiting a clear understanding of the dynamical processes.[15-17] It is therefore desirable to start with simple prototypes and characterise trends with increasing coordination in a bottom-up approach.[14,18]

Here, we present a frequency-resolved photoelectron spectroscopy study of monomer, dimer, and trimer radical anions of *para*-toluquinone (methyl-*para*-benzoquinone, pTQ). The minimum energy structures of these species are shown in Fig. 1. We chose to study cluster anions of pTQ rather the non-methylated *para*-benzoquinone (pBQ) because pTQ anions π-stack readily in the gas-phase at room temperature,[4,19] whereas $(pBQ)_2^-$ is thought to have a non-π-stacked structure.[20] The experimental methodology, frequency-resolved photoelectron spectroscopy, involves recording a series of photoelectron spectra across a wide range of photon energies (*hν*), which, when considered holistically, provide fingerprints of the resonances and their associated dynamics.[7,9,21]

Resonances are quasi-bound excited states embedded in the detachment continuum that form temporary anions through a combination of electron exchange, polarization, and centrifugal forces.[1,2,22,23] For pTQ^-, the excess electron in the ground electronic state resides in a π* orbital, allowing photoexcitation to π*-resonances. Broadly, electronic resonances can have shape [S] or Feshbach [F] character. For a shape resonance, an extra electron occupies an unfilled valence orbital of the neutral ground electronic state configuration, while Feshbach resonances have their corresponding neutral core in an electronic excited configuration.[22]

The frequency-resolved spectra typically have contributions from multiple electron detachment channels:[7-13] (i) direct photodetachment corresponding to instantaneous electron ejection; (ii) prompt autodetachment, in which a resonance is photoexcited and promptly autodetaches the excess electron before significant nuclear rearrangement occurs; (iii) delayed

[a] Department of Chemistry, Durham University, Durham DH1 3LE, United Kingdom. Email: j.r.r.verlet@durham.ac.uk
[b] School of Chemistry, University of Melbourne, Parkville, Melbourne VIC 3010, Australia. Email: james.bull@eigenket.org

† Electronic Supplementary Information (ESI) available: photodetachment yield spectra for pTQ^- and $(pTQ)_3^-$; global fit results for pTQ^-; summary of photodetachment angular distributions for pTQ^-; all frequency-resolved photoelectron spectra for pTQ^- and $(pTQ)_3^-$. See DOI: 10.1039/x0xx00000x

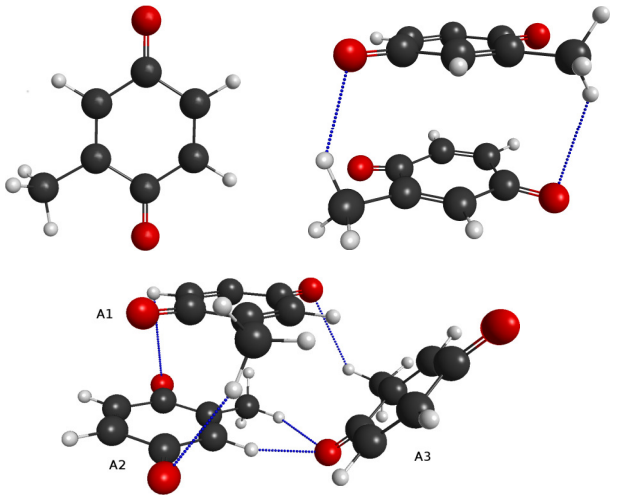

Fig. 1: Illustration of the *para*-toluquinone monomer, dimer and trimer anions. For the dimer, the excess electron is localised on the upper (planar) monomer. The lower (non-planar) monomer has the carbonyl (C=O) groups bent out of the ring plane by ~10°. The trimer equilibrium geometry, taken from Ref. 4, has the excess electron is localised on monomer A3. Key: charcoal – carbon; red – oxygen; white – hydrogen; blue dashed – hydrogen bonds.

autodetachment (DA), where an initial photoexcited resonance is populated for a longer duration before autodetaching or internally converting to a lower-lying resonance that subsequently autodetaches; (iv) vibrational autodetachment (VAD) from a valence or non-valence excited state; and (v) thermionic emission (TE), in which a vibrationally-hot but ground electronic state statistically ejects an electron on the nanosecond to microsecond timescale. The direct photodetachment and prompt autodetachment contributions, (i) and (ii), are jointly referred to as prompt detachment (PD), and are indistinguishable in the frequency-resolved spectrum, although can be inferred through their photoelectron angular distributions.[9,13] DA produces a distribution at lower electron kinetic energy (eKE) due to conversion of photoexcitation energy into nuclear motion, while VAD and TE have characteristic low eKE photoelectron distributions, reflecting their quasi-statistical or statistical nature. Due to the range of possible detachment channels, combined with the fact that photoexcitation of π*-resonances and their associated dynamics can be more probable than direct photodetachment,[7-12] frequency-resolved photoelectron spectroscopy is a useful technique to fingerprint the dynamics of resonances. The method is complementary to 2D electron energy loss spectroscopy,[9,24] with a key advantage that the system under study is charged, allowing mass-selection of the reactant (crucial for cluster studies).

In the present paper we show pTQ^- exhibits above-threshold resonances and associated dynamics similar to those for pBQ^-, although with subtle differences. The dimer, $(pTQ)_2^-$ is susceptible to photodissociation in competition with electron loss, which is more probable than direct photodetachment over at least the first 0.5 eV into the detachment continuum. The trimer, $(pTQ)_3^-$, revealed efficient formation of a non-valence correlation-bound state and vibration-mediated autodetachment up to ~0.7 eV above-threshold. The study provides a striking example of the variety and complexity of dynamics and electron detachment channels available to π*-resonances of small cluster anions.

Experimental

Experiments were performed using a photoelectron velocity-map imaging spectrometer that has been described in detail elsewhere.[7,25] Briefly, a ~2 mM solution of >99% purity pTQ (Sigma-Aldrich) dissolved in analytical grade methanol was electrosprayed at –5 kV and transferred *via* a capillary into an RF ring-electrode ion trap. Ions were thermalised to ~300 K in the trap, allowing formation of a statistical ensemble of cluster isomers.[4] The trapped ions were unloaded into a co-linear time-of-flight optics assembly, accelerating the ion packet along a 1.3 m flight region towards a continuous-mode velocity-mapping (VMI) assembly.[26,27]

Light pulses were generated by a Nd:YAG pumped (Continuum Surelite II-10) optical parametric oscillator (Continuum Horizon I), and timed to interact with the mass-selected ion packet at the centre of the VMI stack. Ejected electrons were velocity-mapped onto a dual multichannel plate (MCP) detector and a P43 phosphor screen assembly; the output was monitored with a CCD camera. Velocity-map images were collected at various wavelengths between $h\nu$ = 4.13 eV (300 nm) and $h\nu$ = 1.88 eV (660 nm), in 5 nm, 10 nm or 20 nm increments. The light had pulse energy of 2 – 3 mJ, and was unfocused to minimise multiphoton contributions. Each velocity-map image accumulated sufficient counts to achieve a comparable signal-to-noise ratio. All images were accumulated with a 500 ns MCP gate; systematic delay of the MCP gate in 50 ns steps relative to the light pulse showed that most electron ejection occurred on a < 50 ns timescale regardless of cluster size, suggesting that only a modest amount of thermionic emission occurred.[7,10,28,29]

Photoelectron image reconstructions used a polar onion peeling[30] algorithm, providing photoelectron spectra and angular distributions (see ESI). The photoelectron eKE scale was calibrated from the spectrum of I^- and the velocity-mapping resolution is around 5%.

Results and discussion

Monomer radical anion, pTQ^-

The frequency-resolved spectrum of pTQ^-, shown in Fig. 2(a), consists of 33 area-normalised photoelectron spectra. The $h\nu$ = 3.54 eV (350 nm) photoelectron spectrum is shown in Fig. 2(b) along with fitted contributions from three detachment channels. These contributions were obtained from a global fit of the frequency-resolved spectra to a photodetachment model assuming the minimum number of physically meaningful parameters.[7,8,11] In the global fit, the TE (thermionic emission, red in Fig 2(b)) channel has a Boltzmann-like thermal distribution, peaking near eKE ~ 0 eV.[7,10] The DA (delayed autodetachment, green in Fig 2(b)) channel has the same (fixed) eKE for all $h\nu$ and a spectral shape consistent with the Wigner threshold law near eKE ~ 0 eV.[31] The PD channel (prompt

detachment, blue in Fig 2(b)) has an eKE distribution that increases linearly with *hv* and agrees with a calculated Franck-Condon direct detachment spectrum.[8] From the global fit of the PD channel, the adiabatic detachment energy (ADE) and vertical detachment energy (VDE) were determined to be 1.8±0.1 eV and 2.1±0.1 eV, respectively. For comparison, the values for pBQ^- are 1.82±0.06 and 1.99±0.04.[8]

The weights of each detachment channel in the global fit are proportional to their relative contribution to the photoelectron spectrum. These weights are shown in Fig. 2(c) as a function of *hv*. Fig. 2(c) has been truncated to *hv* ~ 2.5 eV because the fit cannot reliably distinguish PD and DA channels at lower *hv*. For comparison, Fig. 2(c) also includes fit results from the frequency-resolved spectrum of pBQ^- (dashed lines).[9,32] Overall, the frequency-resolved spectra of pTQ^- are similar to those for pBQ^-, although pTQ^- appears to have a slightly increased PD yield and reduced TE yield.[8] It should also be noted that, while TE appears as a minor channel in Fig. 2, our VMI experiments only capture a small amount (few percent) of the actual TE yield due to a 500 ns gating window on the VMI detector (TE operates on a microsecond timescale).[7,10] Nevertheless, the differences between pTQ^- and pBQ^- are meaningful because the rate of TE will be similar for both systems due to their similar electron affinities and electronic structure.[28,29]

From Fig. 2(c), the dominance of the DA channel in the 2.6 < *hv* < 3.5 eV range is similar to pBQ^-. For pBQ^-, the DA channel was assigned to dynamics occurring on the $^2A_u[S]$ ($1^2[S]$ for pTQ^-) and $2^2B_{3u}[F]$ ($2^2[F]$ for pTQ^-) resonances, which show broad (~0.5 eV) and overlapping Franck-Condon profiles.[9,33] The DA channel has a spectral distribution fixed in eKE, with the peak eKE in good agreement with the calculated energy for the $1^2[S]$ resonance.[7] For *hv* > 3.1 eV, the $2^2[F]$ resonance is available; the corresponding $2^2B_{3u}[F]$ resonance for pBQ^- was shown to internally convert to the lower-lying shape resonance on a ~30 fs timescale,[32] followed by autodetachment on a similar timescale. Overall, it appears the π*-resonance dynamics for pTQ^- parallel those for pBQ^-, except for a small blue shift (~0.1 eV) for pTQ^-.

Despite the close similarity in DA yield for pTQ^- and pBQ^-, there is a clear difference in the yield of the TE channel. The reduced TE yield for pTQ^- suggests ground state recovery is less efficient. Interestingly, the reduction in TE yield for pTQ^- is accompanied by an increase in relative PD yield, but no change to the DA channel yield. As noted earlier, the PD channel contains contributions from both direct photodetachment into the continuum and very fast autodetachment from any photoexcited resonances. Because cross-sections for resonance photoexcitation and direct photodetachment are likely to be very similar for pTQ^- and pBQ^-, any differences in detachment channel contributions will reflect changes in dynamics. That the DA channel yield with *hv* is near identical for pBQ^- and pTQ^- suggests the $2^2[F] \rightarrow 1^2[S]$ conical intersection seam in pTQ^- is just as readily accessed as the corresponding $2^2B_{3u}[F] \rightarrow {}^2A_u[S]$ conical intersection in pBQ^-.[32,34] The difference in TE yield between the two systems may result from an additional decay route directly from the $2^2[F]$ resonance to the ground state;[32] such a conical intersection was identified for pBQ^-, involving

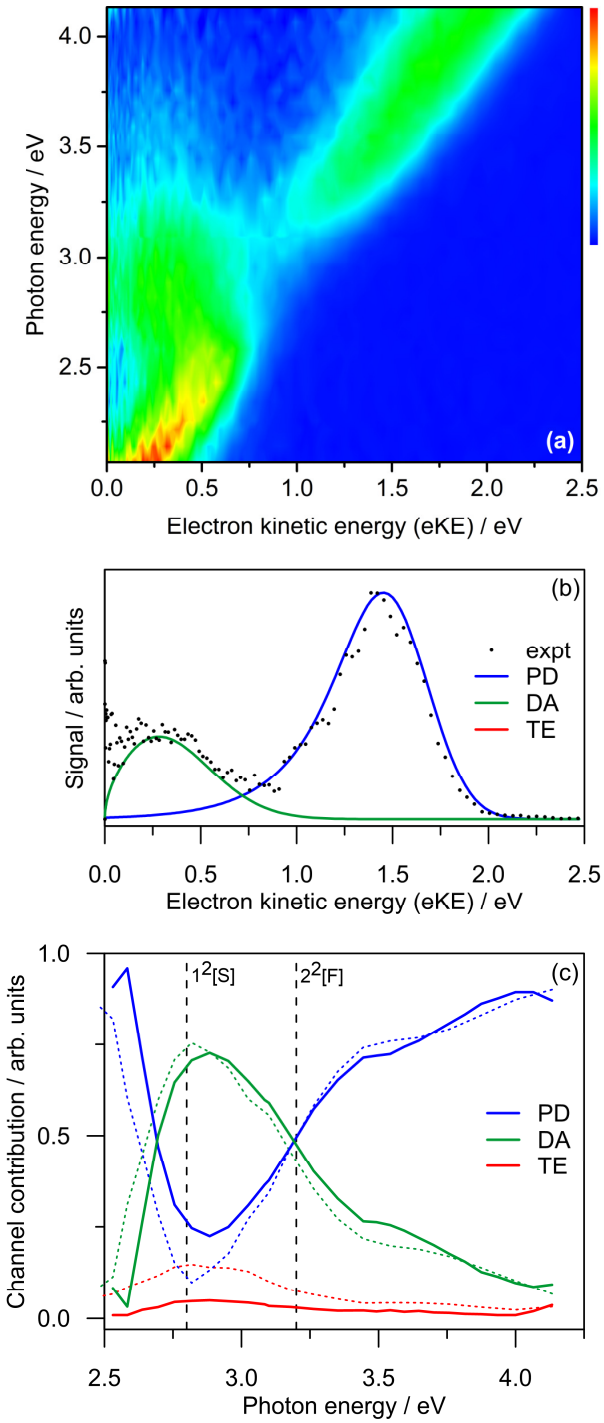

Fig. 2: (a) Frequency-resolved photoelectron spectrum of pTQ^- (each individual spectrum is area-normalised), (b) *hv* = 3.54 eV (350 nm) spectrum with fitted detachment channels and (c) contributions of each electron detachment channel from a global fit of (a). Included in (c) are fitted detachment channel contributions for the pBQ^- frequency-resolved spectrum (short dashed lines) taken from Ref. 8. Vertical lines are calculated energies of two optically active π*-resonances from Ref. 7. Key: PD – prompt detachment, DA – delayed autodetachment, TE – thermionic emission.

symmetric out-of-plane deformation, but was considered to be improbable on the ultrafast timescales of the observed dynamics.[32] For pTQ^-, the methyl-group may hinder these motions due to the additional mass and symmetry breaking, inhibiting direct internal conversion and thus reducing the TE yield. Hence, this additional

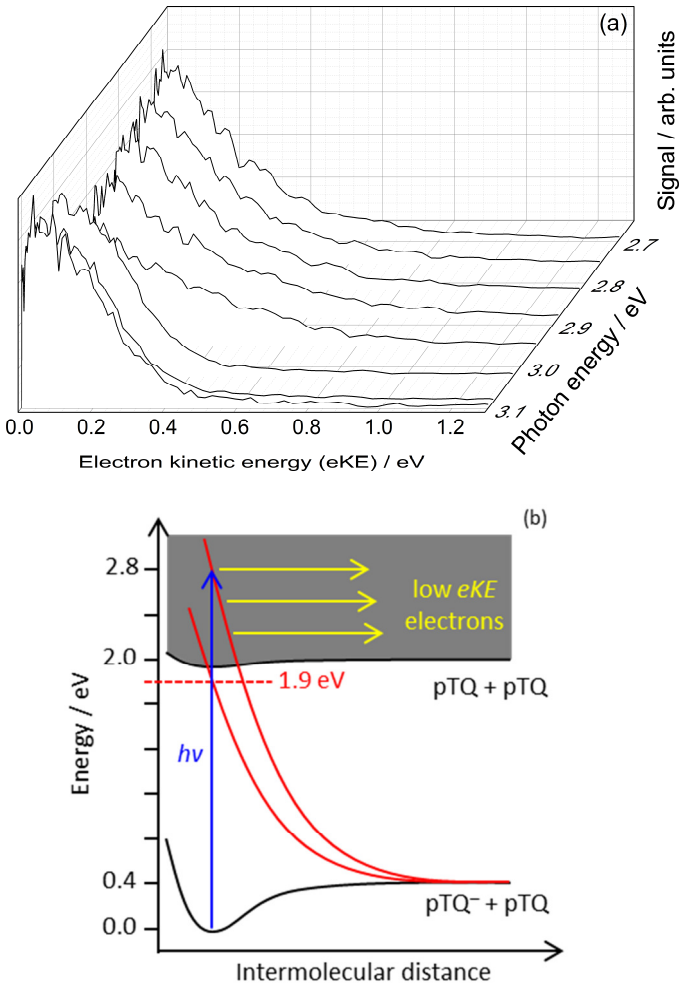

Fig. 3: (a) Photoelectron spectra of $(pTQ)_2^-$ (each spectrum is area normalised), (b) schematic representation of the mechanism leading to the low eKE electrons observed in (a) as a function of the dissociative coordinate. The value of 1.9 eV is the vertical excitation energy for the charge-resonance transition from Ref. 19.

decay route may be accessible, although additional studies on a series of substituted *para*-quinones are needed to explore the importance of this internal conversion pathway.

Dimer radical anion, $(pTQ)_2^-$

The dimer radical anion, $(pTQ)_2^-$, could be generated using electrospray ionisation, although with a low yield. A series of photoelectron spectra are shown in Fig. 3(a), which all show Boltzmann-like distributions at low eKE ($0 \leq$ eKE ≤ 0.4 eV). In the $2.6 \leq h\nu \leq 3.1$ eV range, there is a weak shoulder increasing in eKE commensurate with $h\nu$, consistent with direct detachment. From the $2.6 \leq h\nu \leq 3.1$ eV spectra in Fig. 3(a), the ADE and VDE of $(pTQ)_2^-$ were determined to be 2.1±0.1 eV and 2.5±0.2 eV, respectively. These are ~0.4 eV larger than those for pTQ^- and reflect the cluster cohesion energy.

The equilibrium geometry of $(pTQ)_2^-$, calculated at the ωB97X-D//aug-cc-pVDZ level of theory using Gaussian 09,[35-37] is shown in Fig. 1. At the equilibrium geometry, the two monomers are not geometrically equivalent; the upper monomer has a planar *para*-quinone ring, while the lower monomer has the carbonyl (C=O) groups bent ~10º out of the *para*-quinone ring plane. A similar situation was characterised for the π-stacked $(CQ_0)_2^-$ system.[11] Mulliken population analysis (NBO in parentheses)[38] suggest the upper and lower monomers in Fig. 1 to have charges of –0.83 (–0.84) and –0.17 (–0.16), respectively, implying the excess charge is predominantly localised on the planar monomer, which is solvated by the second non-planar monomer. Comita and Brauman[19] reached the same conclusion through analysis of vibrational structure from a photodissociation spectrum of $(pTQ)_2^-$. Specifically, they identified a charge-resonance state, with a vertical excitation energy of ~1.9 eV, situated just below the detachment threshold. The charge-resonance state corresponds to photoexcitation of the electron from the planar monomer to the non-planar monomer, facilitated by the distorted π-stacking interaction.

The prompt detachment feature in Fig. 3(a) is no longer apparent for $h\nu > 3.0$ eV, suggesting photoexcitation of a resonance and efficient excited state dynamics. While the low-eKE feature in Fig. 3(a) has the appearance of TE, delay of the MCP detector gate relative to the light pulse showed that all electrons were ejected within 50 ns,[10] inconsistent with the microsecond timescale of TE and thus suggesting a different mechanism.

In the present experiments, photodissociation for $h\nu \geq 3.0$ eV was observed,[‡] suggesting the low-eKE feature may result from autodetachment from a dissociative state. This result is consistent with Comita and Braumann:[19] in addition to the band at $h\nu \sim 1.9$ eV, they identified an intense dissociative band producing pTQ^- with onset at $h\nu \sim 2.7$ eV. Given that photodissociation for $(pTQ)_2^-$ must be competitive with the < 50 ns timescale of electron detachment, we assign the Boltzmann-like photoelectron distribution to delayed autodetachment. Specifically, electron loss can occur along a region of the intermolecular coordinate between the monomers as summarised in Fig. 3(b). As energy becomes partitioned into bond breaking, the energy available for the autodetachment is reduced leading the low eKE distribution. This process is analogous to the dynamics of dissociative electron attachment, except initiated here by photoexcitation. However, it is unclear from our experiments whether dissociation occurs directly on the resonance potential energy surface, or whether there is a fast internal conversion to the lower-lying charge resonance state, which then dissociates. Note, the charge resonance state is not purely repulsive by virtue of the vibrational structure seen in the action spectrum of Comita and Brauman.[19]

In summary, the competition between photodissociation and delayed autodetachment determines the appearance of the $(pTQ)_2^-$ photoelectron spectra. Time-resolved photoelectron spectroscopy may prove useful to probe the mechanistic details and timescale of

[‡]Photodissociation of $(pTQ)_2^-$ was observed in the time-of-flight spectra due to ions being deflected off-axis onto a multichannel plate detector after the VMI spectrometer. This short deflection/acceleration region acts as a partial secondary time-of-flight stage (albeit with poor resolution), demonstrating a splitting of the $(pTQ)_2^-$ mass arrival time peak, consistent with photodissociation. Because the ion transit time between the VMI region and deflector is ~1 μs, photodissociation must occur on a sub-microsecond timescale.

dissociation, but these experiments were unsuccessful because of the low parent ion yield.

Trimer radical anion, $(pTQ)_3^-$

The trimer radical anion, $(pTQ)_3^-$, was generated with high abundance from our electrospray source. The 36 area normalised frequency-resolved photoelectron spectra are shown in Fig. 4(a). The $h\nu$ = 4.10 eV (300 nm) spectrum is shown in Fig. 4(b) along with fitted contributions from PD (blue), DA (green), and VAD (red) detachment channels following a similar procedure as for the monomer.[4,11] Detachment channel contributions as a function of $h\nu$ from a three-channel photodetachment model are shown in Fig. 4(c). From the global fit, the ADE and VDE were 2.5±0.1 eV and 3.3±0.2 eV, respectively, which have increased by 0.4 eV and 0.8 eV compared with the dimer. Previous calculations of the $(pTQ)_3^-$ geometry found a distorted π-stacked structure shown in Fig. 1 as the global minimum energy structure.[4] Much like the dimer anion, the charge is localised on one monomer (A3), which is solvated by the other two monomers (A1 and A2).

Fig. 4(a) shows vibrational autodetachment (VAD) to be the predominant electron detachment channel for $h\nu < 3.3$ eV. The VAD channel is associated with a low-eKE distribution, which is identical across all spectra, and shows clear signatures of vibrational structure (see individual spectra in the ESI). A recent time-resolved photoelectron imaging study on photoexcited $(pTQ)_3^-$ at $h\nu$ = 3.10 eV revealed the VAD channel occurs from a non-valence correlation-bound state bound by ~30 - 100 meV.[4] Photoexcitation at $h\nu$ = 3.10 eV first populates a group of π*-resonances, which internally convert on a sub-50 fs timescale to the non-valence state; direct excitation to the non-valence state is improbable due to a low oscillator strength.[11,39] Overall, these dynamics are similar to those recently determined for the co-enzyme Q_0 dimer radical anion, $(CQ_0)_2^-$, except the VAD channel for $(CQ_0)_2^-$ results from a (non-valence) dipole-bound state rather than a non-valence correlation-bound state.[11] The VAD feature in Fig. 4(a) extends below the ADE due to the thermal energy at 300 K (~600 meV).

Above $h\nu$ ~3.4 eV, the VAD channel contribution plateaus at 5-10%, and probably contains contributions from other channels that lead to low-eKE electrons. For $h\nu \geq 3.1$ eV, PD quickly becomes the dominating detachment channel. The photodetachment yield spectrum given in the ESI suggests the onset of broad photoexcitation bands starting from $h\nu \sim 3.4$ eV. Above $h\nu \sim 3.6$ eV, a DA channel becomes accessible with a peak at eKE ~ 0.25 eV, suggesting internal conversion dynamics in the detachment continuum. Interestingly, the photoelectron spectra in this range have the overall appearance of the monomer, except blue-shifted by ~1 eV, which is consistent with the cohesion energy of the cluster, and suggests monomer-like dynamics. Again, these dynamics parallel that observed for $(CQ_0)_2^-$, pointing to a common set of excited state dynamics in *para*-quinone cluster anions. While calculation to assign resonances for $(pTQ)_3^-$ leading to the PD and DA channels are too demanding to be considered in the present study, calculations performed as part of our earlier time-resolved study revealed two groups of resonances centred at 3.36 – 3.48 eV and 3.65 – 3.71 eV, respectively,[4] consistent with the observation in Fig. 4(a) of resonance dynamics occurring in the $3.1 \leq h\nu \leq 4.2$ eV range.

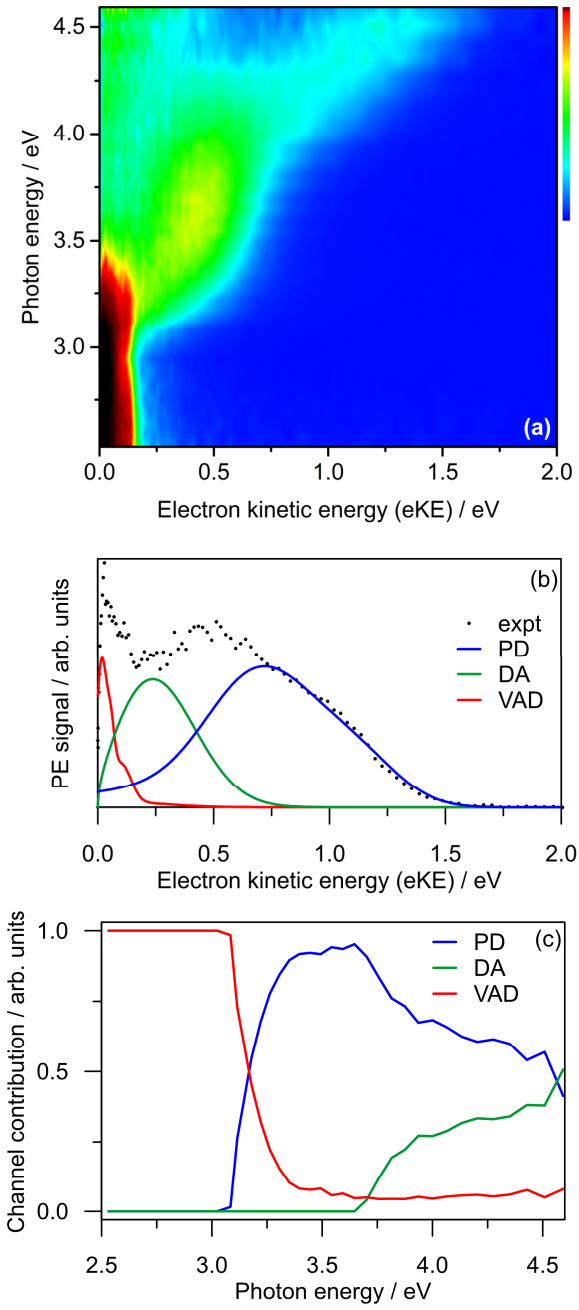

Fig. 4: (a) Frequency-resolved photoelectron spectrum of $(pTQ)_3^-$, (b) $h\nu$ = 4.10 eV (300 nm) spectrum and fitted detachment channels and (c) contributions of each electron detachment channel from the global fit. Key: VAD – vibrational autodetachment; DA – delayed autodetachment; PD – prompt detachment.

Evolution of resonance dynamics with cluster size

Anion cluster studies in the gas phase have shown that structures and electronic properties can be highly sensitive to size, particularly for clusters consisting of a few sub-units.[14,40-43] The present study provides an intriguing example of highly specific cluster/microsolvation excited state dynamics for size-selected pTQ cluster anions. While the frequency-resolved spectra show evidence of monomer-like dynamics for $(pTQ)_3^-$, strong interaction between the charged monomer and neighbouring neutral monomers leads to new decay channels. For example,

dissociation is the major channel for $(pTQ)_2^-$, while internal conversion to a non-valence state becomes available for $(pTQ)_3^-$, apparently outcompeting dissociation. The present study highlights the number of possible decay channels available for resonances in anionic molecular clusters can increase rapidly, many of which are in direct competition. We expect that much larger clusters of pTQ will have multiple low-energy cluster geometries, which may exhibit unique resonance dynamics. For example, some cluster geometries may support non-valence dipole-bound states.[3] Due to the lack of experimental data on the dynamics of excess electrons localized in resonances for small cluster species, it is difficult to compare the present cluster anions with wider literature. However, it is clear that further studies on the dynamics of π*-resonances across a range of anionic clusters and, ideally, selected cluster geometries, would be a useful future direction. For example, characterising the point at which the dynamics extrapolate to bulk can provide molecular level insight into condensed-phase electron capture and transport dynamics. For pTQ, it would be interesting to investigate whether photoexcitation of resonances in larger clusters leads to formation of non-valence correlation-bound states,[4] which resemble pre-solvated or conduction-band electrons in bulk pTQ.

Conclusions

Frequency-resolved photoelectron spectra of monomer, dimer and trimer radical anions of pTQ have been reported. In all cases, multiple electron detachment channels contribute to the photoelectron spectra in the first ~1 eV window above threshold. The monomer radical anion has photoelectron spectra with fingerprints of π*-resonances that parallel those for *para*-benzoquinone anion (pBQ^-). However, subtle differences in thermionic emission yield point to a competing direct decay pathway between the first bright Feshbach resonance and the electronic ground state, which is more efficient for pBQ^- than for pTQ^-. The dimer anion shows a combination of photodissociation and delayed autodetachment. Direct photodetachment appears to be a minor detachment channel up to at least 0.5 eV above threshold. The trimer anion shows formation and vibrational autodetachment from a non-valence correlation-bound state situated just below the detachment threshold. At higher photon energies, there is a combination of prompt detachment and delayed autodetachment. The dynamics at higher photon energies appear consistent with monomer dynamics, blue-shifted in *hν* by the cluster cohesion energy.

Overall, these three pTQ anion systems highlight the variety of non-adiabatic dynamics available to π*-resonances and the profound changes that occur with clusterization. Our work illustrates the versatility of frequency-resolved photoelectron spectroscopy for probing excited state dynamics and electron driven chemistry of small cluster anions. With a suitable cluster source, the frequency-resolved photoelectron spectroscopy technique can, in principle, be applied to much larger mass-selected clusters (tens to hundreds of monomer units). This approach may allow extrapolation of resonances dynamics towards the bulk while still retaining molecular level insights.

Acknowledgements

Funding was provided by the ERC (Starting Grant 306536). We thank Christopher West for experimental assistance.

References

1. J. Simons, *J. Phys. Chem. A*, 2008, **112**, 6401.
2. K. D. Jordan and P. D. Burrow, *Chem. Rev.*, 1987, **87**, 557.
3. K. D. Jordan and F. Wang, *Annu. Rev. Phys. Chem.*, 2003, **54**, 367.
4. J. N. Bull and J. R. R. Verlet, *Sci. Adv.*, 2017, **3**, e1603106.
5. M. Ehara and T. Sommerfeld, *Chem. Phys. Lett.*, 2012, **537**, 107.
6. T. C. Jagau and A. I. Krylov, *J. Chem. Phys.*, 2016, **144**, 054113.
7. J. N. Bull, C. W. West and J. R. R. Verlet, *Chem. Sci.*, 2015, **6**, 1578.
8. J. N. Bull, C. W. West and J. R. R. Verlet, *Phys. Chem. Chem. Phys.*, 2015, **17**, 16125.
9. C. W. West, J. N. Bull, E. Antonkov and J. R. R. Verlet, *J. Phys. Chem. A*, 2014, **118**, 11346.
10. J. N. Bull, C. W. West and J. R. R. Verlet, *Phys. Chem. Chem. Phys.*, 2015, **17**, 32464.
11. J. N. Bull, C. W. West and J. R. R. Verlet, *Chem. Sci.*, 2016, **7**, 5352.
12. C. W. West, J. N. Bull, A. S. Hudson, S. L. Cobb and J. R. R. Verlet, *J. Phys. Chem. B*, 2015, **119**, 3982.
13. L. H. Stanley, C. S. Anstöter and J. R. R. Verlet, *Chem. Sci.*, 2017, **8**, 3054.
14. X.-B. Wang, *J. Phys. Chem. A*, 2017, **121**, 1389.
15. R. D. Levine. *Molecular Reaction Dynamics;* Cambridge University Press, 2009.
16. N. E. Henriksen and F. Y. Hansen. *Theories of Molecular Reaction Dynamics: The Microscopic Foundation of Chemical Kinetics;* Oxford University Press, 2012.
17. P. L. Houston. *Chemical Kinetics and Reaction Dynamics;* Dover Publications, 2006.
18. V. G. Stavros and J. R. R. Verlet, *Annu. Rev. Phys. Chem.*, 2016, **67**, 211.
19. P. B. Comita and J. I. Brauman, *J. Am. Chem. Soc.*, 1987, **109**, 7591.
20. S. K. Lim, M. E. Burba and A. C. Albrecht, *J. Phys. Chem.*, 1994, **98**, 9665.
21. C. S. Anstöter, J. N. Bull and J. R. R. Verlet, *Int. Rev. Phys. Chem.*, 2016, **35**, 509.
22. H. S. Taylor, G. V. Nazaroff and A. Golebiewski, *J. Chem. Phys.*, 1966, **45**, 2872.
23. J. Simons and K. D. Jordan, *Chem. Rev.*, 1987, **87**, 535.
24. K. Regeta and M. Allen, *J. Chem. Phys.*, 2015, **142**, 184307.
25. J. Lecointre, G. M. Roberts, D. A. Horke and J. R. R. Verlet, *J. Phys. Chem. A*, 2010, **114**, 11216.
26. D. A. Horke, G. M. Roberts, J. Lecointre and J. R. R. Verlet, *Rev. Sci. Instrum.*, 2012, **83**, 063101.
27. A. T. J. B. Eppink and D. H. Parker, *Rev. Sci. Instrum.*, 1997, **68**, 3477.
28. E. E. B. Campbell and R. D. Levine, *Annu. Rev. Phys. Chem.*, 2000, **51**, 65.
29. J. U. Andersen, E. Bonderup and K. Hansen, *J. Phys. B*, 2002, **35**, R1.
30. G. M. Roberts, J. L. Nixon, J. Lecointre, E. Wrede and J. R. R. Verlet, *Rev. Sci. Instrum.*, 2009, **80**, 053104.
31. E. P. Wigner, *Phys. Rev.*, 1948, **73**, 1002.
32. D. A. Horke, Q. Li, L. Blancafort and J. R. R. Verlet, *Nat. Chem.*, 2013, **5**, 711.
33. A. A. Kunitsa and K. B. Bravaya, *Phys. Chem. Chem. Phys.*, 2016, **18**, 3454.
34. A. A. Kunitsa and K. B. Bravaya, *J. Phys. Chem. Lett.*, 2015, **6**, 1053.
35. J.-D. Chai and M. Head-Gordon, *Phys. Chem. Chem. Phys.*, 2008, **10**, 6615.

36. T. H. Dunning, Jr., *J. Chem. Phys.*, 1989, **90**, 1007.

37. M. J. Frisch, G. W. Trucks, H. B. Schlegel, G. E. Scuseria, M. A. Robb, J. R. Cheeseman, G. Scalmani, V. Barone, B. Mennucci, G. A. Petersson, H. Nakatsuji, M. Caricato, X. Li, H. P. Hratchian, A. F. Izmaylov, J. Bloino, G. Zheng, J. L. Sonnenberg, M. Hada, M. Ehara, K. Toyota, R. Fukuda, J. Hasegawa, M. Ishida, T. Nakajima, Y. Honda, O. Kitao, H. Nakai, T. Vreven, Jr., J. A. Montgomery, J. E. Peralta, F. Ogliaro, M. Bearpark, J. J. Heyd, E. Brothers, K. N. Kudin, V. N. Staroverov, R. Kobayashi, J. Normand, K. Raghavachari, A. Rendell, J. C. Burant, S. S. Iyengar, J. Tomasi, M. Cossi, N. Rega, N. J. Millam, M. Klene, J. E. Knox, J. B. Cross, V. Bakken, C. Adamo, J. Jaramillo, R. Gomperts, R. E. Stratmann, O. Yazyev, A. J. Austin, R. Cammi, C. Pomelli, J. W. Ochterski, R. L. Martin, K. Morokuma, V. G. Zakrzewski, G. A. Voth, P. Salvador, J. J. Dannenberg, S. Dapprich, A. D. Daniels, Ö. Farkas, J. B. Foresman, J. V. Ortiz, J. Cioslowski and D. J. Fox. *Gaussian, Inc.;* Wallingford CT, 2009.

38. A. E. Reed, R. B. Weinstock and F. Weinhold, *J. Chem. Phys.*, 1985, **83**, 735.

39. M. L. Theis, A. Candian, A. G. G. M. Tielens, T. J. Lee and R. C. Fortenberry, *Phys. Chem. Chem. Phys.*, 2015, **17**, 14761.

40. T. Maeyama, Y. Negishi, T. Tsukuda, I. Yagia and N. Mikami, *Phys. Chem. Chem. Phys.*, 2006, **8**, 827.

41. R. M. Young, M. A. Yandell, M. Niemeyer and D. M. Neumark, *J. Chem. Phys.*, 2010, **133**, 154312.

42. R. M. Young, G. B. Griffin, A. Kammrath, O. T. Ehrler and D. M. Neumark, *Chem. Phys. Lett.*, 2010, **485**, 59.

43. R. M. Young and D. M. Neumark, *Chem. Rev.*, 2012, **112**, 5553.